Simultaneous Occurrence of Structure-Directed and Particle-Resonance-Induced Phononic Gaps in Colloidal Films

T. Still,[1] W. Cheng,[1] M. Retsch,[1] R. Sainidou,[2] J. Wang,[1,3] U. Jonas,[1,3] N. Stefanou,[4] and G. Fytas[1,3,*]

[1]*Max Planck Institute for Polymer Research, Ackermannweg 10, 55128 Mainz, Germany*
[2]*Instituto de Óptica-CSIC, Serrano 121, 28006 Madrid, Spain*
[3]*Department of Materials Science, University of Crete and FORTH, 71110 Heraklion, Greece*
[4]*Section of Solid State Physics, University of Athens, Panepistimioupolis, 15784 Athens, Greece*

(Received 26 November 2007; revised manuscript received 3 April 2008; published 13 May 2008)

We report on the observation of two hypersonic phononic gaps of different nature in three-dimensional colloidal films of nanospheres using Brillouin light scattering. One is a Bragg gap occurring at the edge of the first Brillouin zone along a high-symmetry crystal direction. The other is a hybridization gap in crystalline and amorphous films, originating from the interaction of the band of quadrupole particle eigenmodes with the acoustic effective-medium band, and its frequency position compares well with the computed lowest eigenfrequency. Structural disorder eliminates the Bragg gap, while the hybridization gap is robust.

DOI: 10.1103/PhysRevLett.100.194301 PACS numbers: 43.20.+g, 61.46.−w, 63.20.D−, 82.70.Dd

Structured materials with a periodic modulation in the density and elastic coefficients, so-called phononic crystals [1], can exhibit phonon band gaps at Bragg frequencies or wavelengths commensurate to their lattice constant. In addition to Bragg gaps (BG), theory predicts gaps evoked by resonance modes of the constituent components interacting with the extended acoustic branch of the composite structure [2]. These gaps prevent elastic waves with certain frequencies to propagate through the crystal at least in certain crystallographic directions. The width and the position of the BG in general depends on the contrast between the densities (ρ), longitudinal and transverse sound velocities (c_l and c_t) of the component materials, and on the lattice parameter [3–5]. Yet, structures with strong localized resonant elements can shift the gap well below the Bragg frequency associated to the lattice constant [6,7]. Soon after the first experimental observation of ultrasonic band gaps [8–12], peculiar phenomena with potential applications dealing with the propagation of elastic waves in periodic composite materials such as tunneling [13], negative refraction, focusing [14,15], and enhanced transmission through one-dimensional gratings [16] have been discovered. Most realized systems deal so far with sonic and ultrasonic phononic crystals with periodicity in the millimeter range [6,7,9–15]. To shift the gap to higher frequencies [17], the creation of periodic patterns at the submicron scale is necessary, which can benefit from techniques currently explored for the fabrication of structures in soft matter [18]. Recently, we have adopted a colloidal self-assembly technique [19] by vertical lifting deposition to fabricate fcc films of monodisperse polystyrene (PS) spheres on glass substrates with subsequent fluid infiltration. The phononic dispersion relation of such a single crystalline pattern measured by spontaneous Brillouin light scattering (BLS) led to the first observation of a hypersonic BG along high-symmetry crystallographic directions [20]. By varying the particle size and the infiltrated fluid, the hypersonic frequency and the width of the gap could be tuned. More recently, a hypersonic BG was also observed in two-dimensional structures fabricated by optical lithography [21].

In soft opals, the spherical particles represent local resonant elements, and hence the bands, which originate from the multipole modes of these interacting particles, can overlap with the acoustic field of the extended states in the effective medium. As a result of this hybridization, a gap opens up in the vicinity of the eigenfrequency of the quadrupole particle modes [2], which we refer to as hybridization gap (HG). Such gaps originate, in general, from level repulsion when two bands of the same symmetry cross each other, about the crossing point. An optical analogue of this gap is encountered, e.g., in metallodielectric photonic crystals, as a result of hybridization between collective particle-plasmon modes and the extended effective-medium band [22]. Albeit there was a hint of HG in colloidal suspensions [23–26], its demonstration, assignment and the concurrent observation along with the BG has been missing. Here, we report on the first, to the best of our knowledge, realization of a double phononic gap in fcc colloidal crystals formed by colloidal self-assembly during vertical lifting deposition with subsequent fluid infiltration. The effect of the elastic contrast between the fluid matrix and solid inclusions as well as the crystalline order of the structure on the two gaps is distinct. Furthermore, in amorphous colloidal glasses, only the HG persists.

The fabrication of the colloidal films starts with the deposition of the particles by vertically lifting a glass substrate from the aqueous colloid suspension [19]. For different experiments, two kinds of monodisperse polystyrene (PS) spheres with diameters of $d = 307$ nm and 360 nm and poly(methylmethacrylate) (PMMA) particles

with a diameter of $d = 327$ nm were used for the fabrication of the fcc opals. Additionally, a noncrystalline hybrid film consisting of PS sphere mixture with two different diameters (300 and 360 nm) was prepared in the same way. After complete drying, the films were infiltrated with liquid poly(dimethylsiloxane) (PDMS) and any liquid excess was blown off. By this method, uniform wet colloidal films with a thickness of about 10 μm were obtained. The phononic dispersion relation was measured by BLS for the dry and liquid infiltrated state of these films. BLS probes the thermal phonon propagation in the sample along a selected direction determined by the scattering geometry [20]. For the given experimental conditions, the scattering wave vector of the photon lies in the (111) plane of the fcc lattice, and its amplitude $q = (4\pi/\lambda)\sin(\theta/2)$ depends on the scattering angle θ and the wavelength of the incident laser beam λ. At low q values for which the system appears homogeneous, the wave vector of the phonon $\mathbf{k}$ and that of the inelastically scattered light $\mathbf{q}$ are equal. Under these conditions, the BLS spectrum at a given q consists of a doublet with a Doppler frequency shift $\omega = \pm ck$, where c is the speed of sound with longitudinal (or transverse) polarization in the effective medium (e.g., lowest spectrum in Fig. 2).

The precursor dry PS and PMMA opals have a highly ordered crystalline morphology as indicated by the scanning electron microscope (SEM) image in Fig. 1. The single crystalline order extends over a few hundred μm. The dry films exhibit strong multiple light scattering due to the large optical contrast between the particles and the surrounding air and due to the particles elastic form factor. The wave vector $\mathbf{q}$ is, therefore, ill-defined which precludes the measurement of the dispersion relation $\omega(\mathbf{q})$. Nonetheless, the BLS spectrum of the dry opals reveals several localized (q-independent) modes [27,28]. These are identified as vibration eigenmodes of the particles, and each mode can be specified by a pair of indices (i, l) defining the l-th spherical harmonic of the i-th radial mode in analogy to the atomic orbitals [28]. The frequencies of these sphere eigenmodes depend on the size of the particle, the mass density and the speed of sound in air, and in the particle for both polarizations (i.e., compression and shear moduli). Consequently, the mechanical properties of the samples can be reliably determined from the theoretical fit of the experimental eigenfrequencies. The obtained longitudinal and transverse sound velocities in the two types of particle materials along with the lowest $f(1,2)$ eigenfrequency are given in Table I. For the particles embedded in the infiltrated PDMS, the eigenfrequencies can be theoretically [26,29] computed using the elastic parameters of Table I. Expectedly, $f(1,2)$ decreases when the spheres are embedded in PDMS.

The infiltration of the thin dry opals by PDMS with a refractive index ($n = 1.45$) close to that of the PS particles ($n = 1.59$) diminishes multiple light scattering, and hence $\mathbf{q}$ is well defined. To obtain the desired dispersion relation $\omega(\mathbf{q})$, the BLS spectra of the wet opals were recorded along the high-symmetry directions of the reciprocal space. In the present case of the fcc lattices, the first Brillouin zone (BZ) is a truncated octahedron. The experimental $\mathbf{q}$ is confined in the hexagon formed by the intersection of the (111) plane with the BZ [20]. The direction of $\mathbf{q}$ is selected along Γ–M, where M is the edge center of the hexagon and the evolution of the BLS spectra with $\mathbf{q}$ near the BZ for the PS wet opal is shown in Fig. 2. The simple picture of single phonon propagation in the effective medium at low q values becomes complex as q increases towards the BZ boundary. Up to four Lorentzian curves are required to

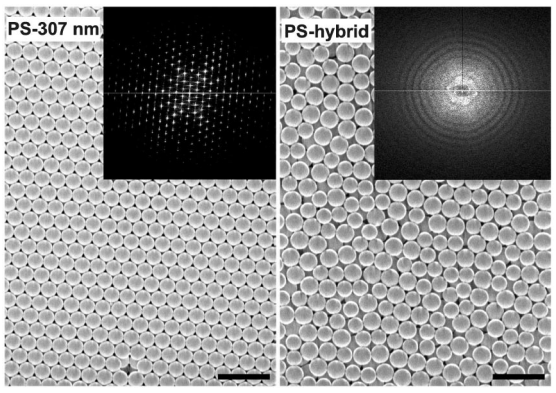

FIG. 1. SEM top-view images of the PS-307 crystal (left) and the PS-hybrid (right)—both "dry" before infiltration (scale bar is 1 μm). The insets display the Fourier-transform images computed from the SEM pictures over an area of about 4 μm by 4 μm.

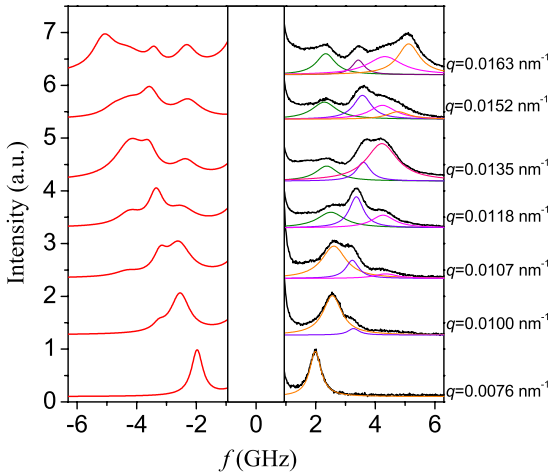

FIG. 2 (color online). BLS spectra of the wet opal of PS spheres with diameter 307 nm in a PDMS matrix at different wave vectors in the (111) plane of the fcc crystalline colloidal film. The edge of the BZ along the probed direction corresponds to $q_{BZ} \approx 0.013$ nm^{-1}. The deconvolution in different spectral components is indicated for the Stokes side of the spectrum, and the representation of the experimental spectra by the superposition of these Lorentzian lines is shown for the anti-Stokes side. Each spectrum is normalized to the total integrated intensity, for comparison of the relative contributions.

TABLE I. Sound velocities, particle sizes, and lowest eigenfrequencies in colloid-based phononics. [densities ρ (kg/m^3): PS: 1050, PMMA: 1190, PDMS: 965].

Material	c_t (ms^{-1})	c_l (ms^{-1})	d (nm)	$f(1,2)$ (GHz)	c ms^{-1}
PS	1200 ± 30	2350 ± 50	307	3.3[a]	
			360	2.9[a]	
PDMS	0	1050 ± 20[a]			
PS-PDMS		1670 ± 30[a]	307	2.2[b]	1490[b]
		1570 ± 30[a]	360	1.9[b]	1490[b]
Hybrid-PDMS		1510 ± 20[a]	300/360		1400[b,c]
PMMA	1400 ± 40	2800 ± 50	327	4.0[a]	
PMMA-PDMS		1720 ± 30[a]	327	2.3[b]	1560[b]

[a]Measured by BLS. [b]Computed for the wet opals. [c]for 65% filling fraction of spheres.

represent the experimental BLS spectrum. In contrast to the PS–silicon oil opal [20] with a single peak splitting across the BZ boundary, the same opal infiltrated in PDMS providing higher elastic contrast displays richer spectral features and exhibits a second splitting at lower q values within the first BZ. The experimental dispersion relation is depicted in Fig. 3. In the hypersonic PS-PDMS crystal ($d = 307$ nm) only one longitudinal phonon branch is observed at low q values with $c = 1670$ ms^{-1}, intermediate between the longitudinal sound velocities in the pure component materials. Transverse phonons are not observed experimentally, probably because PDMS cannot support shear waves and the mechanical contact between the particles is weakened. The most striking feature of the dispersion diagram is the simultaneous presence of two band gaps at about 3 and 4 GHz, respectively. The latter is clearly a BG since it occurs at the edge of the BZ, $q = q_{BZ} \approx 0.0133$ nm^{-1}, that matches the distance Γ–M, i.e., $(3/2)^{3/2}\pi/a$, where $a = \sqrt{2}d$ is the lattice constant of the given fcc crystal. An analogue behavior is observed in the second wet opal of the larger PS spheres ($d = 360$ nm) for which the gap positions shift to lower wave vectors and frequencies (open circles in the upper left diagram of Fig. 3).

In order to elucidate further the nature of the two gaps, we examined the effect of the crystalline order on the experimental band diagram. The formation of a hybrid colloidal film consisting of a mixture of an equal number of two PS spheres ($d = 300$ nm and $d = 360$ nm) artificially broadens the size distribution beyond the polydispersity limit of about 5% necessary for crystallization [30]. Indeed, the crystallization is prohibited in this hybrid colloidal film, as indicated by the lack of a long-range order in the right-hand panel of Fig. 1, leading to an amorphous colloidal glass. The BLS spectra of the infiltrated monodisperse opal and hybrid films are shown in Fig. 4 for two wave vectors. The deletion of one peak in the spectrum of the hybrid is due to the disappearance of the BG in the disordered hybrid, as it is clearly shown in the dispersion plot in the upper left diagram of Fig. 3 (solid squares). Apparently, the crystalline order is a prerequisite

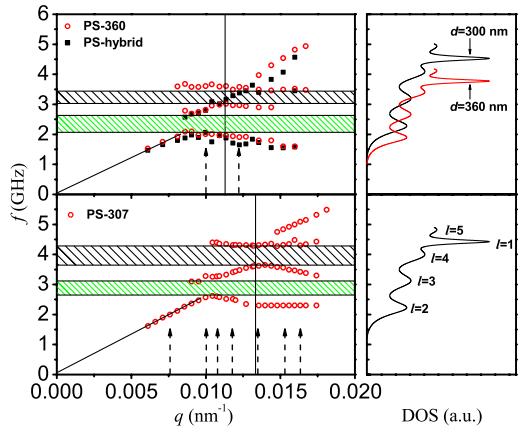

FIG. 3 (color online). Phononic band diagrams for the different PS wet opals under consideration, along the Γ–M direction (see text). The hatched bands mark the phononic gaps, and the vertical arrows indicate the q values in the corresponding spectra of Fig. 2 and 4 below. The vertical lines denote the first BZ limit (for $d = 307$ nm and $d = 360$ nm, respectively). The change in the DOS induced by the corresponding single PS particle in PDMS is shown in the right-hand panel.

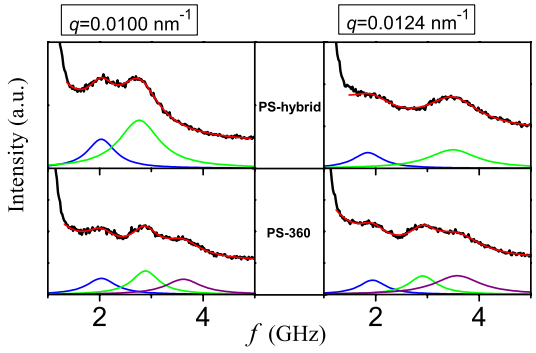

FIG. 4 (color online). Exemplary BLS spectra of the PS ($d = 360$ nm)/PDMS wet opal (bottom) and the wet PS-hybrid colloidal film (top) at two q values indicated by the arrows in the corresponding diagram of Fig. 3. The deconvolution into different spectral components is shown below each spectrum (note the absence of the BG-induced spectral features in the hybrid).

for the BG but not for the newly observed lower frequency HG, which is omnidirectional in the colloidal glass. An identification of the latter as a theoretically anticipated HG [2], through density-of-states (DOS) calculations [29], is examined in Fig. 3. The right-hand panel of Fig. 3 displays several eigenmodes of the individual PS spheres embedded in the fluid PDMS. The lowest $f(1, 2)$ appears to compare well with the frequency at the crossing with the acoustic branch and the opening of the HG. Moreover, the lowest frequency points at the experimental dispersion at high q's compare very well with the computed $f(1, 2)$. This and the two higher flat bands of localized modes in Fig. 3 cause sufficiently strong inelastic light scattering at high q's [26] and compare well with the particle resonances of higher l. Their presence in the BLS spectra obscures the resolution of the phonons in the second BZ. Interestingly, the bands originating from particle resonant modes appear to be considerably narrower and occur at higher frequency than theoretically predicted [2]. This can be ascribed to viscous losses in the liquid matrix that were not taken into account in the theoretical calculations, and which weaken the interparticle interactions as a result of the reduced overlap between the corresponding wave fields. Qualitatively, the opening of the two gaps is also observed in a third wet opal of PMMA with $d = 327$ nm in PDMS [31]. The HG occurs at 2.5 GHz, very close to the $f(1, 2) = 2.35$ GHz of this particle in PDMS, whereas the wet opal exhibits a sound velocity of 1720 ± 30 ms^{-1} in the long-wavelength limit (Table I).

It is worth noting that the various effective-medium theories (EMT) [32] yield sound velocities about 10% smaller than the experiment, even if the viscosity in the liquid matrix is taken into account. On the other hand, if we consider the colloidal film as a polymer (solid) matrix with fluid inclusions, EMT [32] strongly overestimates the sound velocity. The above, in view also of the fact that measured sound velocities agree generally well with the results of EMT in non close-packed colloidal crystals [33], suggests the existence of consolidation, at least to some degree that may be different for different samples, in the colloidal films [34]. This also explains why the measured effective sound velocity is different in the two PS-PDMS crystals (see Table I).

In conclusion, we discovered, for the first time, two phononic band gaps of different nature coexisting at hypersonic frequencies in the same physical system and elucidated the underlying physical mechanisms. Induced disorder did not destroy the newly demonstrated HG. This study has been possible by taking advantage of the opportunities offered by the colloidal science to tailor the phononic band diagram of nanostructured materials, measured directly by BLS. Manipulating the flow of phonons may allow heat management, e.g., in thermoelectrics. Finally, we pointed out the need of a detailed quantitative evaluation of the dispersion diagrams of colloid-based phononic structures, by means of full elastodynamic calculations that take into account consolidation and soft matter properties (e.g. structural dynamics of the component materials or interfacial effects), which still remains an open challenging theoretical problem.

M. R. thanks the VCI e.V for financial support. Partial financial support from the EU (SoftComp) is gratefully acknowledged.

*fytas@mpip-mainz.mpg.de

[1] T. Gorishnyy *et al.*, Phys. World **18**, 24 (2005).
[2] I. E. Psarobas *et al.*, Phys. Rev. B **65**, 064307 (2002).
[3] J. Baumgartl, M. Zvyagolskaya, and C. Bechinger, Phys. Rev. Lett. **99**, 205503 (2007).
[4] M. Sigalas and E. N. Economou, Solid State Commun. **86**, 141 (1993).
[5] M. S. Kushwaha *et al.*, Phys. Rev. Lett. **71**, 2022 (1993).
[6] Z. Liu *et al.*, Science **289**, 1734 (2000).
[7] C. Goffaux *et al.*, Phys. Rev. Lett. **88**, 225502 (2002).
[8] R. Martínez-Sala *et al.*, Nature (London) **378**, 241 (1995).
[9] F. R. Montero de Espinoza, E. Jimenez, and M. Torres, Phys. Rev. Lett. **80**, 1208 (1998).
[10] J. V. Sánchez-Pérez *et al.*, Phys. Rev. Lett. **80**, 5325 (1998).
[11] Z. Liu *et al.*, Phys. Rev. B **62**, 2446 (2000).
[12] J. O. Vasseur *et al.*, Phys. Rev. Lett. **86**, 3012 (2001).
[13] S. Yang *et al.*, Phys. Rev. Lett. **88**, 104301 (2002).
[14] X. D. Zhang and Z. Y. Liu, Appl. Phys. Lett. **85**, 341 (2004).
[15] S. Yang *et al.*, Phys. Rev. Lett. **93**, 024301 (2004).
[16] M.-H. Lu *et al.*, Phys. Rev. Lett. **99**, 174301 (2007).
[17] T. Gorishnyy *et al.*, Phys. Rev. Lett. **94**, 115501 (2005).
[18] J.-H. Jang *et al.*, Nano Lett. **6**, 740 (2006).
[19] C. A. Fustin *et al.*, Langmuir **20**, 9114 (2004).
[20] W. Cheng *et al.*, Nat. Mater. **5**, 830 (2006).
[21] T. Gorishnyy *et al.*, Appl. Phys. Lett. **91**, 121915 (2007).
[22] V. Yannopapas, A. Modinos, and N. Stefanou, Phys. Rev. B **65**, 235201 (2002).
[23] J. Liu *et al.*, Phys. Rev. Lett. **65**, 2602 (1990).
[24] L. Ye *et al.*, Phys. Rev. E **48**, 2805 (1993).
[25] X. Jing, P. Sheng, and M. Zhou, Phys. Rev. Lett. **66**, 1240 (1991).
[26] R. S. Penciu *et al.*, J. Chem. Phys. **118**, 5224 (2003).
[27] M. H. Kuok *et al.*, Phys. Rev. Lett. **90**, 255502 (2003).
[28] R. S. Penciu *et al.*, Phys. Rev. Lett. **85**, 4622 (2000).
[29] R. Sainidou *et al.*, Z. Kristallogr. **220**, 848 (2005).
[30] S.-E. Phan *et al.*, J. Chem. Phys. **108**, 9789 (1998).
[31] See EPAPS Document No. E-PRLTAO-100-020820. The figure contains the dispersion diagram measured by Brillouin light scattering of the PMMA 327 nm particles, mentioned in our Letter, after infiltration with PDMS. Related density-of-states calculations are also appended. For more information on EPAPS, see http://www.aip.org/pubservs/epaps.html.
[32] A. H. Harker and J. A. G. Temple, J. Phys. D **21**, 1576 (1988); G. C. Gaunaurd and W. Wertman, J. Acoust. Soc. Am. **85**, 541 (1989).
[33] G. Tommaseo *et al.*, J. Chem. Phys. **126**, 014707 (2007).
[34] D. L. Johnson and T. J. Plona, J. Acoust. Soc. Am. **72**, 556 (1982).